



Porphyromonas gingivalis infection alters microRNA composition in extracellular vesicles

Kayo Yoshida^a, Kaya Yoshida^{a,*}, Yasuhiro Mouri^b, Ayu Takai^a, Mariko Seyama^a, Mana Mekata^a, Noriko Mizusawa^b, Keiko Miyoshi^b, Yasusei Kudo^b, Kazumi Ozaki^a

^a Department of Oral Healthcare Promotion, Tokushima University Graduate School of Biomedical Sciences, 3-18-15, Kuramoto, Tokushima, 770-8504, Japan

^b Department of Oral Bioscience, Tokushima University Graduate School of Biomedical Sciences, 3-18-15, Kuramoto, Tokushima, 770-8504, Japan

ARTICLE INFO

Keywords:

Periodontal disease
microRNA
Macrophage
Extracellular vesicle
Porphyromonas gingivalis

ABSTRACT

Objectives: Periodontitis, commonly associated with *Porphyromonas gingivalis* (Pg), involves intricate alterations of oral intercellular interactions, in which extracellular vesicles (EVs) play a pivotal role. The understanding of the miRNA profiles in the EVs derived from Pg-infected cells (Pg-EVs) remains incomplete despite acknowledging their importance in intercellular communication during periodontitis. Therefore, our objective was to identify and characterize the miRNAs enriched in Pg-EVs.

Methods: Microarray analysis was conducted to examine the miRNA profiles in the EVs derived from Pg-infected THP-1 cells. We compared the identified miRNAs with those upregulated in the EVs after stimulation with LPS. Additionally, we explored how inhibiting TLR signaling during Pg infection affects the transcription of specific miRNAs. We investigated the unique sequence motifs specific to the miRNAs concentrated in Pg-EVs.

Results: The levels of eleven miRNAs, including miR-155, were increased in Pg-EVs compared with those elevated after LPS stimulation. The Pg-induced miR-155 upregulation via TLR2 but not TLR4 signaling suggests the influence of TLR signaling on the miRNA composition of EVs. Furthermore, the miRNAs upregulated in Pg-EVs contained AGAGGG and GRGGSGC sequence motifs.

Conclusions: Our findings demonstrate that Pg-induced alterations in EV-containing miRNA composition occur in a TLR4-independent manner. Notably, the concentrated miRNAs in Pg-EVs harbor specific motifs with a high G + C content within their sequences. The upregulation of specific miRNAs in EVs under infectious conditions suggests the influence of both innate immune receptor signals and miRNA sequence characteristics.

1. Introduction

Periodontal disease is a chronic inflammatory condition commonly associated with *Porphyromonas gingivalis* (Pg), a gram-negative anaerobic bacterium frequently found in the oral cavity, although other bacteria such as *Treponema denticola* can also contribute to the disease. Recent single-cell RNA-seq analyses have revealed alterations in the interactions between stromal and immune cells within the gingival mucosa of patients with periodontitis [1]. Recognition of bacterial components by innate immune receptors expressed in both stromal and immune cells may initiate intercellular interactions [1].

Exosomes secreted by infected stromal and immune cells have been identified as modulators of innate immune responses [2]. Extracellular vesicles (EVs), including exosomes, are membrane-bound vesicles released by cells into the extracellular environment. These EVs carry diverse biomolecules, such as proteins, lipids, RNA, and DNA, facilitating their transfer to recipient cells and influencing intercellular communication and various biological processes, including inflammation and immune responses. EVs derived from Pg-infected cells have been linked to inflammation and disease pathogenesis [3]. The modulation of the innate immune response by EVs is believed to contribute to the intricate intercellular communication observed in periodontal

Abbreviations: Pg, *Porphyromonas gingivalis*; EVs, extracellular vesicles; miRNAs, microRNAs; LPS, lipopolysaccharide; FBS, fetal bovine serum; PMA, phorbol myristate acetate; NMWL, nominal molecular weight limit; SD, standard deviation.

* Corresponding author. 3-18-15, Kuramoto, Tokushima, 770-8504, Japan.

E-mail addresses: c302141001@tokushima-u.ac.jp (K. Yoshida), kaya@tokushima-u.ac.jp (K. Yoshida), ymouri@tokushima-u.ac.jp (Y. Mouri), c302331002@tokushima-u.ac.jp (A. Takai), seyama.mariko@tokushima-u.ac.jp (M. Seyama), c302231002@tokushima-u.ac.jp (M. Mekata), mizusawa@tokushima-u.ac.jp (N. Mizusawa), miyoshi@tokushima-u.ac.jp (K. Miyoshi), yasusei@tokushima-u.ac.jp (Y. Kudo), ozaki@tokushima-u.ac.jp (K. Ozaki).

<https://doi.org/10.1016/j.job.2024.04.001>

Received 17 December 2023; Received in revised form 2 April 2024; Accepted 2 April 2024

Available online 4 April 2024

1349-0079/© 2024 Japanese Association for Oral Biology. Published by Elsevier B.V. All rights reserved.

diseases.

EVs encapsulate various components that can initiate inflammation, such as bacterial elements and host-derived histones [4]. MicroRNAs (miRNAs) among components of EVs play pivotal roles in regulating gene expression in recipient cells. Ranging from 20 to 25 nucleotides in length, miRNAs interact with multiple mRNA sequences, impede translational responses, and suppress the expression of diverse genes [5]. While miRNAs typically function within host cells, they are also secreted by EVs [6]. Exosomal miRNAs originating from innate immune cells, such as macrophages or dendritic cells, have been reported to transfer to recipient cells and regulate inflammation by suppressing target genes [7,8].

Several studies have suggested that the miRNA profile in EVs differs significantly from that in host cells [9–11]. Recently, it has been observed that specific sequences within the miRNA sequence determine the sorting of miRNAs into EVs, while distinct sequences are associated with cellular retention. These sorting sequences vary across cell types but commonly exhibit a high G + C content of four to seven nucleotides [9]. Additionally, it has been reported that fluctuations in intracellular target sequences of miRNAs associated with cell activation influence miRNA sorting into EVs [10]. Currently, efforts are underway to identify miRNAs within EVs across various tissues and cell types, including cancer cells. These investigations reveal fluctuations in the composition of EV-containing miRNAs depending on the source of production [12].

While miRNA within EVs has been extensively studied in the context of various inflammatory diseases [13–15], limited research has been conducted on EV-contained miRNAs associated with periodontal disease. Therefore, we comprehensively identified specific miRNAs within EVs produced by macrophage-like cells infected with *Pg*. Upregulated miRNAs within EVs following *Pg* infection are distinctly different from those upregulated into EVs by lipopolysaccharide (LPS) stimulation, arising from the recognition of each pathogen by distinct upstream receptors. Additionally, we investigated the sequence characteristics of the miRNAs enriched in EVs due to *Pg* infection. This study provides a new mechanistic perspective on the alternation of miRNA composition within EVs during *Pg* infection and could aid in identifying novel biomarkers for periodontal disease.

2. Materials and methods

2.1. Bacterial cultures

P. gingivalis ATCC33277 was cultivated in Brain Heart Infusion medium (BD Bioscience, Franklin Lakes, New Jersey, USA), supplemented with 0.5% yeast extract (BD Bioscience), 10 µg/mL hemin (FUJIFILM Wako Pure Chemical Corporation, Osaka, Japan), and 1 µg/mL 2-methyl-1,4-naphthoquinone (vitamin K3) (Tokyokasei, Tokyo, Japan) in an anaerobic jar at 37 °C.

2.2. Cell culture

The human monocytic cell line THP-1 was seeded at a concentration of 30,000 cells/mL and cultured in Roswell Park Memorial Institute (RPMI) 1640 medium (Sigma-Aldrich, by Merck KGaA, Darmstadt, Germany) with 10% fetal bovine serum (FBS) (Gibco by Thermo Fisher Scientific, Waltham, Massachusetts, USA) at 37 °C under a humidified atmosphere containing 5% CO₂.

2.3. Bacterial infection

THP-1 cells were seeded in 10% FBS/RPMI 1640 medium. After 24 h, they underwent differentiation into macrophages through treatment with 100 nM phorbol myristate acetate (PMA) (FUJIFILM Wako Pure Chemical Corporation) for 48 h. Subsequently, the medium was replaced with 2% FBS/RPMI 1640, and the cells were infected with *Pg* (MOI = 100).

For EV extraction, following 4 h of *Pg* infection, any uninternalized bacteria were washed away with PBS. Cells were then cultured in RPMI 1640 medium with a 2% Exo-FBSHI (Exosome-depleted and Inactivated FBS) (System Biosciences, Palo Alto, California, USA) for 48 h. The EVs released into the culture medium were collected. It has been reported that both host cells and intracellular *Pg* remain viable for at least 48 h post-infection [4]. Therefore, we selected the 48-h time point as the most efficient for EV collection.

2.4. EV isolation

EVs were isolated from the culture medium using the polymer-based precipitation method. The enrichment process involved employing Amicon Ultra-15 Centrifugal Filter Device with a nominal molecular weight limit (NMWL) of 100,000 Da (Sigma-Aldrich). For the polymer method, we utilized the Total Exosome Isolation Reagent (Thermo Fisher Scientific). It has been reported that the shape and size (approximately 200 nm) of EVs obtained by this method remained unchanged upon *Pg* infection [4].

2.5. Microarray analysis

EVs were extracted from both *Pg*-infected and non-infected cells, following established protocols. The miRNAs within the EVs were subsequently extracted using 3D-Genes RNA extraction reagent, and their quality was assessed using a 2100 Bioanalyzer (Agilent Technologies, Santa Clara, California, USA). The miRNA samples underwent labeling with the 3D-Genes miRNA Labeling kit and were then subjected to hybridization at 32 °C for 16 h. Microarray analysis was conducted using a Human miRNA Oligo chip (TORAY, Tokyo, Japan) with chip ID SH06R24, along with the 3D-Genes Scanner 3000 (TORAY). To determine the expression level of each miRNA, background values were subtracted from the obtained values. Further global normalization was performed by adjusting the median signal intensity to 25. MicroRNAs with a microarray expression score of less than 100 in non-infected cells, were excluded from downstream analysis.

2.6. mRNA isolation and real-time PCR

The cells were homogenized in ISOGEN (Nippon Gene, Tokyo, Japan), and total RNA extraction was conducted following the manufacturer's protocol. Subsequently, cDNA synthesis was performed using the Prime Script™ RT reagent kit (Takara Bio, Kyoto, Japan). Real-time PCR was carried out with SYBR Premix Ex Taq (Takara Bio) on a 7300 Real-Time PCR system (Applied Biosystems, Carlsbad, CA, USA). The primer sequences used were as follows: human GAPDH (NM_001289745.3): forward, 5'-GCACCGTCAAGGCTGAGAAC-3', reverse, 5'-TGGTGAAGACGCCAGTGA-3'; human β-actin (NM_001101.5): forward, 5'-CATGTACGTTGCTATCCAGGC-3', reverse, 5'-CTCCTTAATGTACGCACGAT-3'; human TBP (NM_003194): forward, 5'-CCACTCACAGACTCTACAAC-3', reverse, 5'-CTGCGGTA-CATCCCAGAACT-3'; human MIR155HG (NR_001458): forward, 5'-GCAGTTTTGGCTTGTTCAT-3', reverse, 5'-AAAACGTTGCCAGCAATCC-3'; human TNF-α (NM_000594): forward, 5'-CCTCTCTAATCAGCCCTCTG-3', reverse, 5'-GAGGACCTGGGAGTAGTAG-3'; human IL-6 (NM_000600): forward, 5'-AAGCCA-GAGCTGTGCAGATGAGTA-3', reverse, 5'-TGTCTGCAGCCACTGGTTC-3'; human IL-10 (NM_000572): forward, 5'-GACTTTAAGGGT-TACCTGGGTTG-3', reverse, 5'-TCACATGCGCCTTGATGTCTG-3'; human CD206 (NM_002438.4): forward, 5'-TTCGGA-CACCCATCGGAATTT-3', reverse, 5'-CACAAGCGCTGCGTGGAT-3'.

The PCR was conducted for 40 cycles with two steps at 95 °C and 60 °C. Each gene's expression was quantified using standard curves. Internal reference genes (β-actin, TBP and GAPDH), which exhibit the most stable expression under each experimental condition, were used for normalization. All data were standardized based on the normalized

expression values of the control samples.

2.7. miRNA isolation and real-time PCR

The cells and EVs were homogenized using ISOGEN II (Nippon Gene), and small RNAs were isolated according to the manufacturer's protocol. Following this, cDNA synthesis and real-time PCR were performed using the miRCURY LNA miRNA PCR Starter Kit (QIAGEN, Hilden, Germany) and the 7300 Real-Time PCR system (Applied Biosystems). The PCR was conducted for 40 cycles with two steps at 95 °C and 56 °C. Each gene's expression was quantified using standard curves. All data were standardized based on the normalized expression values of the control samples.

2.8. Inhibitor treatment

Upon inducing differentiation of THP-1 cells into macrophages, a 30-min pre-treatment was performed using 10 μM TLR2-IN-C29, 10 μM TLR4-IN-C34, or 5 μM BAY 11–7085 (Enzo Life Sciences, Inc, USA) in 2% FBS/RPMI 1640 medium. Subsequently, THP-1 cells were infected with *Pg*, and mRNA was collected 2 h post-infection.

2.9. Immunocytochemistry

THP-1 cells were fixed in 4% formalin for 30 min and permeabilized with 100% methanol for 20 min on ice. Following a 45-min block with 4% BSA/PBS, the cells were incubated overnight at 4 °C with anti-NF-κB p65 antibody (F-6, Santa Cruz Biotechnology, sc-8008) (diluted 1:1000) or normal mouse IgG. Subsequently, Alexa Fluor 566-conjugated anti-rabbit IgG antibody (Thermo Fisher Scientific) (dilution not required) was added for 1 h. Nuclear staining was performed using Hoechst 33342 for 30 min. The samples were observed under a BZ-X800 microscope (Keyence, Osaka, Japan). The ImageJ Fiji software was utilized to segment the nuclear staining images and calculated the average intensity of p65 staining in each nucleus.

2.10. Transcription factor (TF)-miRNA regulation analysis

The regulation of miRNA expression by NF-κB members was analyzed using the TransmiR v2.0 database (<https://www.cuilab.cn/transmir>). In this database, the reliability of TF-miRNA regulation is classified according to the definition of miRNA promoter regions in ChIP-seq analysis. The presence of transcription factor binding sites was depicted as variations in color in [Supplementary Fig. 1](#), based on differences in reliability.

2.11. Calculation of free energy for miRNAs

Free energy of the thermodynamic ensemble was calculated using RNAfold program from each miRNA sequence (<http://rna.tbi.univie.ac.at/cgi-bin/RNAWebSuite/RNAfold.cgi>). miRNA sequences were obtained from the miRBase database (<https://www.mirbase.org/>).

2.12. miRNA motif analysis

The identification of four to seven-base sequence motifs within the miRNAs concentrated in EVs during *Pg* infection was performed using the default settings of the STREME software available at The MEME Suite site (<https://meme-suite.org/>). Sequences generated by shuffling the input sequences were used as controls. Additionally, motif enrichment analysis was conducted using SEA software from the same site, employing the sequences of miRNAs that were downregulated in EVs during *Pg* infection as controls. The search for AGAGGG and GRGGSGC motifs in miR-132 was conducted using the FIMO software from the same site.

2.13. Pathway analysis for target genes of miRNAs

The KEGG pathway for target genes of upregulated miRNAs in EVs following *Pg* infection was analyzed in miRPathDB v2.0 website (<http://mpd.bioinf.uni-sb.de/overview.html>). We analyzed the pathways enriched with experimentally validated miRNA target genes and predicted target genes. We created heatmaps for pathways shared by at least three miRNAs.

2.14. EVs treatment

THP-1 cells were seeded in RPMI 1640 medium supplemented with 10% FBS at a density of 30×10^4 cells/mL. After 24 h, 100 nM PMA was added, and the cells were treated for an additional 48 h to induce differentiation into macrophages. EVs were added at various concentrations, followed by a change in the medium.

2.15. Statistical analysis

Statistical analyses were performed using Statcel4, GraphPad Prism10 software and R environment. The normal distribution of data was initially assessed using the Goodness-of-fit test using the chi-square statistic. Variables exhibiting normal distribution were assessed using Student's t-test for two-group comparison. For multiple-group comparisons, the Tukey-Kramer test was conducted. The significance level was set at p or adjusted $p < 0.05$. To assess the adequacy of sample size for the two-group comparison, we calculated Cohen's d . In most cases, the resulting values were above 2, indicating adequacy [16]. Each experiment was independently conducted at least twice. All data are presented as mean \pm standard deviation (SD).

3. Results

3.1. Identification of miRNAs within EVs derived from *Pg*-infected THP-1 cells

THP-1 macrophage-like cells were infected with *Pg* for 4 h. Subsequently, both *Pg* and EVs were removed from the medium. miRNAs contained within EVs, released from infected cells into the medium within 48 h, were identified using miRNA microarray analysis. In comparison to non-infected cells, 11 miRNAs were upregulated, while 17 were downregulated in EVs from *Pg*-infected cells (*Pg*-EVs) (Table 1). Notably, miR-146a/b and miR-155, recognized the biomarkers for periodontitis [17,18], were significantly upregulated. To validate these findings and address potential microarray bias, we confirmed the increased expression of miR-146a-5p and miR-155-5p in EVs (Fig. 1A) and intracellularly (Fig. 1B) using real-time PCR. Consistent Spike-In expression between infected and non-infected cell-derived EVs validated the accuracy of the RT procedures (Fig. 1A). Considering the role of LPS in innate immunity activation in gram-negative bacteria such as *Pg*, we compared miRNAs increased in *Pg*-EVs with those increased by LPS stimulation [19]. miRNAs affected by LPS stimulation did not exhibit significant changes in *Pg*-EVs (Table 2). This suggests that the alternation of miRNA profile induced by *Pg* infection may be independent of Toll-like receptor 4 (TLR4) signaling.

3.2. Enhanced miR-155 expression via the TLR2/NF-κB pathway in response to *Pg* infection

We hypothesized that, beyond TLR4, other innate immune receptors activated by *Pg* infection might amplify the expression of identified miRNAs. To explore this, we analyzed transcriptional regulation for *MIR155HG*, the host gene of miR-155-5p. Notably, a significant increase in *MIR155HG* expression in THP-1 cells was observed as early as 2 h post-*Pg* infection (Fig. 2A). This elevation in intracellular miR-155 levels persisted for up to 48 h post-infection (Fig. 1B). Given the established

Table 1
miRNAs with substantial variation in EVs derived from Pg-infected THP-1 cells.

Name	sequence	ID	fold change	category
hsa-miR-146a-5p	UGAGAACUGAAUCCAUGGGU	MIMAT0000449	3.13	Pg-up
hsa-miR-3197	GGAGGCGCAGGCUCGAAAGGCG	MIMAT0015082	2.70	Pg-up
hsa-miR-155-5p	UUAUUGCUAAUCGUGAUAGGGU	MIMAT0000646	2.70	Pg-up
hsa-miR-146b-5p	UGAGAACUGAAUCCAUGGGU	MIMAT0002809	2.63	Pg-up
hsa-miR-550a-5p	AGUGCCUGAGGGAGUAAGAGCCC	MIMAT0004800	2.56	Pg-up
hsa-miR-3178	GGGGCGCGCCGGAUCG	MIMAT0015055	2.27	Pg-up
hsa-miR-3616-3p	CGAGGGCAUUUCAUGAUGCAGGC	MIMAT0017996	2.27	Pg-up
hsa-miR-4276	CUCAGUGACUCAUGUGC	MIMAT0016904	2.17	Pg-up
hsa-miR-6807-5p	GUGAGCCAGUGGAAUGGAGAGG	MIMAT0027514	2.08	Pg-up
hsa-miR-671-5p	AGGAAGCCUGGAGGGGCGUGAG	MIMAT0003880	2.08	Pg-up
hsa-miR-642a-3p	AGACACAUUUGGAGAGGGAACC	MIMAT0020924	2.00	Pg-up
hsa-miR-20a-5p	UAAAGUGCUUAUAGUGCAGGUAG	MIMAT0000075	0.50	Pg-down
hsa-miR-3156-5p	AAAGAUUCUGAAGUGGGAGACA	MIMAT0015030	0.48	Pg-down
hsa-miR-4793-5p	ACAUCUGCUCCACAGGGCAGAG	MIMAT0019965	0.47	Pg-down
hsa-miR-5006-5p	UUGCCAGGGCAGGAGUGGAA	MIMAT0021033	0.47	Pg-down
hsa-miR-3135b	GGCUGGAGCGAGUGCAGUGGUG	MIMAT0018985	0.46	Pg-down
hsa-miR-7151-3p	CUACAGGCUGGAAUGGGCUCA	MIMAT0028213	0.44	Pg-down
hsa-miR-4486	GCUGGGCGAGGCUGGCA	MIMAT0019020	0.44	Pg-down
hsa-miR-6865-5p	UAGGUGGCAGAGGAGGGACUUCA	MIMAT0027630	0.43	Pg-down
hsa-miR-6895-5p	CAGGGCCAGGCACAGAGUAAG	MIMAT0027690	0.40	Pg-down
hsa-miR-6778-5p	AGUGGGAGGACAGGAGGCAGGU	MIMAT0027456	0.36	Pg-down
hsa-miR-5008-3p	CCUGUGCUCGCCAGGGCCUCGC	MIMAT0021040	0.33	Pg-down
hsa-miR-4648	UGUGGGACUGCAAUUGGGAG	MIMAT0019710	0.31	Pg-down
hsa-miR-6131	GGCUGGUCAGAUGGGAGUG	MIMAT0024615	0.30	Pg-down
hsa-miR-3937	ACAGGGCGCUGUAGCAAUGGGGG	MIMAT0018352	0.29	Pg-down
hsa-miR-670-5p	GUCCUGAGUGUAUUGUGGUG	MIMAT0010357	0.26	Pg-down
hsa-miR-6834-5p	GUGAGGGACUGGGAUUUGUGG	MIMAT0027568	0.25	Pg-down
hsa-miR-6073	GGUAGUGAGUUAUCAGCUAC	MIMAT0023698	0.18	Pg-down

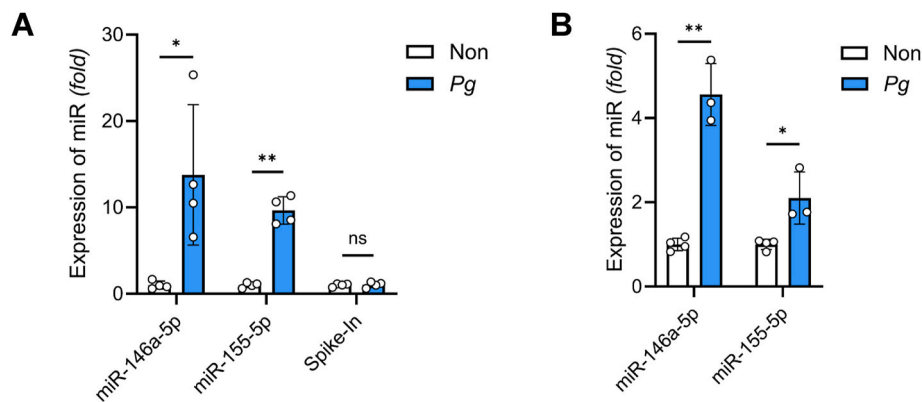
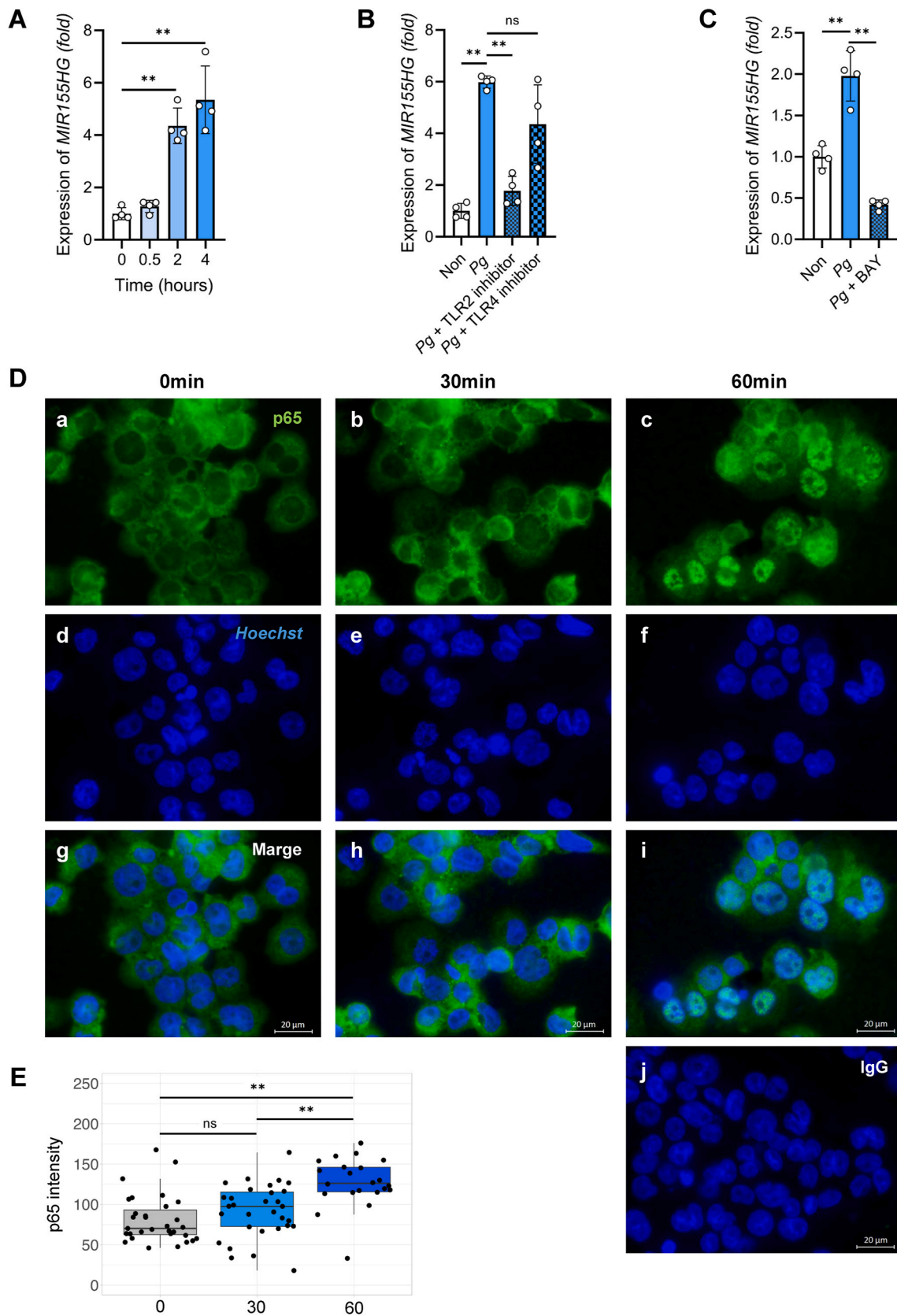


Fig. 1. Upregulated expression levels of miR-146a-5p and miR-155-5p in EVs and intracellularly due to *Pg* infection. **(A)** The expression levels of miR-146a-5p and miR-155-5p were assessed in EVs derived from the *Pg*-infected (*Pg*) and non-infected (*Non*) THP-1 cells using real-time PCR. EVs released into the medium for 48 h after infection were collected. Spike-In serves as a control for RNA samples and RT reactions, allowing for a direct readout of assay success and identification of poor-quality samples. Data are shown as mean ± standard error of the mean from four biological replicates (n = 4). *p < 0.05, **p < 0.01. The values of d for miR-146 and miR-155 are 2.218 and 7.5876, respectively. **(B)** The expression levels of intracellular miR-146a-5p and miR-155-5p 48 h after *Pg* infection from four biological replicates (n = 4). miR-103 levels were used to normalize miRNA expression levels. *p < 0.05, **p < 0.01. The values of d for miR-146 and miR-155 are 4.0576 and 1.991, respectively.

Table 2
miRNAs, reported as LPS sensitive miRNAs, in EVs derived from *Pg*-infected cells.

Name	sequence	ID	fold change	category
hsa-miR-103a-3p	AGCAGCAUUGUACAGGGCUAUGA	MIMAT0000101	1.39	LPS-up
hsa-miR-4479	CGCGGGCCGUGCUCGGAGCAG	MIMAT0019011	1.18	LPS-up
hsa-miR-1307-5p	UCGACCGGACCUCGACCGGCU	MIMAT0022727	1.14	LPS-up
hsa-miR-423-5p	UGAGGGGCAGAGGCGAGACUUU	MIMAT0004748	1.10	LPS-up
hsa-miR-3605-3p	CCUCCGUGUUAUCCUGUCCUCUAG	MIMAT0017982	0.85	LPS-up
hsa-miR-590-5p	GAGCUUAUUCUAUAAAAGUCAG	MIMAT0003258	1.27	LPS-down
hsa-miR-629-5p	UGGGUUUACGUUGGGAGACU	MIMAT0004810	1.18	LPS-down
hsa-miR-103b	UCAUAGCCCUGUACAAGUCUGCU	MIMAT0007402	1.14	LPS-down
hsa-miR-6774-3p	UCGUGUCCCUUUGUCCACAG	MIMAT0027449	1.11	LPS-down
hsa-miR-210-3p	CUGUGCGUGGACAGCGGCUGA	MIMAT0000267	0.92	LPS-down
hsa-miR-589-3p	UCAGAACAAAUGCCGGUCCCGA	MIMAT0003256	0.77	LPS-down



(caption on next page)

Fig. 2. TLR2/NF- κ B dependent upregulation of *MIR155HG* expression levels in THP-1 cells due to *Pg* infection (A) *MIR155HG* expression levels in THP-1 cells were assessed at various time points (0, 0.5, 2, 4 h) after *Pg* infection using real-time PCR. The data represent the mean \pm standard error of the mean from four biological replicates ($n = 4$). β -actin levels were used to normalize mRNA expression levels. ** adjusted $p < 0.01$, compared to THP-1 cells with *Pg* added at 0 h. (B) THP-1 cells, pretreated with TLR2/4 inhibitors, were infected with *Pg*, and *MIR155HG* expression levels were assessed 2 h after infection using real-time PCR. Data are presented as mean \pm standard error of the mean from four biological replicates ($n = 4$). TBP levels were used to normalize mRNA expression levels. ** adjusted $p < 0.01$. (C) THP-1 cells, pretreated with the NF- κ B inhibitor BAY, were infected with *Pg* and *MIR155HG* expression levels were assessed 2 h after infection using real-time PCR. Data are presented as mean \pm standard error of the mean from four biological replicates ($n = 4$). TBP levels were used to normalize mRNA expression levels. ** adjusted $p < 0.01$. (D) The translocation of the p65 subunit to the nucleus in THP-1 cells was assessed at different time points after *Pg* infection. The staining for the p65 subunit was performed using a p65 antibody (a, b, c) or normal rabbit IgG (j). Nuclei were counterstained with Hoechst 33342 (d, e, f), and then the resulting microscopic images (g, h, i) were merged. Imaging was conducted using the Keyence BZ-X800 all-in-one microscope. (E) The boxplot depicts the brightness of p65 staining per unit area in the nucleus of each cell determined by Hoechst staining. ** adjusted $p < 0.01$.

role of TLR2 in *Pg* recognition [20–22], we examined the impact of TLR2 signaling on *MIR155HG* transcription. Pre-treatment with a TLR2 inhibitor (TLR2-IN-C29) attenuated *Pg*-induced *MIR155HG* expression, while a TLR4 inhibitor (TLR4-IN-C34) showed no effect (Fig. 2B).

TLR2 ligands typically activate NF- κ B. Correspondingly, NF- κ B p50/65 directly binds to and activates the human *MIR155HG* proximal promoter in certain cells [23]. The NF- κ B inhibitor, BAY, reversed the enhanced *MIR155HG* expression induced by *Pg* infection (Fig. 2C). Immunohistochemistry revealed nuclear translocation of phosphorylated p65 in THP-1 cells after 60 min post-*Pg* infection, preceding the upregulation of *MIR155HG* expression (Fig. 2A and D).

We investigated whether the expression of miRNAs altered in *Pg*-EVs is regulated by NF- κ B signaling through in silico analysis. Among the upregulated miRNAs, seven miRNAs including miR-155 contain p65 binding sequences in their promoters, while seven out of the down-regulated miRNAs also harbor p65 binding sequences in their promoters (Supplemental Fig. 1).

3.3. Selective enrichment of miRNAs with specific motifs in EVs during *Pg* infection

During *Pg* infection, certain miRNAs, such as miR-146 and miR-155, exhibit increased intracellular expression, potentially influencing their amounts into EVs (Figs. 1B and 2A). Previous studies have reported a >10-fold increase in the intracellular expression of miR-132 and miR-146 in THP-1 macrophage-like cells shortly after *Pg* infection [24]. The enhanced expression of miR-132 was suppressed by simultaneous inhibition of TLR2/TLR4 [24], corroborating our observations (Fig. 2B). However, our microarray data did not reveal a significant increase in miR-132 expression within *Pg*-EVs (miR-132-3p: 1.59-fold increase; miR-132-5p: 1.05-fold increase). The composition of miRNAs in EVs is presumed to be influenced by factors such as the sequence characteristics of miRNAs and the activation status of host cells [9–11]. We postulate that, among the miRNAs demonstrating cellular-level increases due to *Pg* infection, those harboring specific molecular characteristics based on the sequence that contribute to miRNA stability and/or sorting might be selectively enriched within EVs. To investigate this, we first investigated the GC contents and free energy, which associate with miRNA stability and/or sorting [9,25]. There were no differences in GC content or free energy between the mature miRNAs that increased and decreased in *Pg*-EVs (Supplemental Fig. 2). Additionally, we explored common sequence motifs among the miRNAs concentrated in *Pg*-EVs using STREME software (Fig. 3). All four detected motifs were present in 27.3% of the miRNAs, particularly the AGAGGG and GRGGSGC motifs, which exhibited high G + C content within five–seven nucleotides, resembling reported miRNA sorting sequences [9]. Due to the limited number of input sequences, accurate p-value calculations could not be performed. Furthermore, in comparison to the miRNAs that were downregulated in *Pg*-EVs, the concentrated miRNAs demonstrated notably higher motif enrichment. Importantly, these high G + C motifs were not detected in the miR-132 sequence.





Motif	P value	% EVs-miRNA	miRNA	Enrichment Ratio
	0.11	27.3	hsa-mir-642a-3p hsa-mir-3616-3p hsa-mir-155-5p	10.5
	0.11	27.3	hsa-mir-642a-3p hsa-mir-3178 hsa-mir-155-5p	9.00
	0.11	27.3	hsa-mir-3178 hsa-mir-3197 hsa-mir-671-5p	7.50
	0.11	27.3	hsa-mir-550a-5p hsa-mir-4276 hsa-mir-6807-5p	6.75

Fig. 3. Putative sorting motif within the upregulated miRNAs in EVs from *Pg*-infected cells

The four motif sequences detected within the sequences of 11 upregulated miRNAs in EVs derived from *Pg*-infected cell were shown. P-values were calculated using control sequences, which consisted of randomly shuffled sequences generated from the input sequences. The enrichment ratio was calculated by comparing the 11 upregulated miRNAs in EVs from *Pg*-infected cells with the 17 miRNAs that decreased in EVs derived from *Pg*-infected cells.

3.4. Inferred functions of upregulated miRNAs within EVs from *Pg*-infected cells

miRNAs sharing common sequence motif may be considered to have functional associations. Pathway analysis was conducted for the target genes of miRNAs upregulated within *Pg*-EVs. While target genes of miR-146/155, supported by experimental evidence, were found to be enriched in pathways related to inflammation and immune response, such as TNF, TLR, BCR, TCR signaling pathway, and others, no enrichment in pathways was observed for the target genes of the remaining miRNAs (Supplemental Fig. 3A). *Pg*-EVs reduced the expression of IL-10 in non-infected recipient cells (Supplemental Fig. 4). Analysis using miRNet (<https://www.mirnet.ca/>) revealed that among the upregulated miRNAs, miR-155-5p and miR-671-5p, which possess the high G + C motif, were predicted to target IL-10 (data not shown).

Pathway analysis was also conducted on predicted target genes of miRNAs. The analysis revealed enrichment in pathways related to ErbB signaling and endocytosis, among others (Supplemental Fig. 3B). The ErbB signaling pathway is considered crucial in mucosal immune responses to infection [26]. This suggests that miRNAs such as miR-642a and miR-3616 which possess the AGAGGG motif may potentially regulate oral mucosal immunity. Overall, these results suggest that miRNAs involved in inflammation and mucosal immunity may harbor functional motifs that facilitate their secretion.

4. Discussion

The study represents the first comprehensive identification of

miRNAs present in *Pg*-EVs. Among the 11 miRNAs upregulated in *Pg*-EVs, miR-146a/b and miR-155 are well-documented as miRNAs associated with periodontitis [17,18,27] and known to play a role in inflammation [8]. The expression of miR-146 and miR-155 has been reported to be enhanced by innate immune receptor signaling [28,29], supporting our observations. While some studies have conducted transcriptome analyses of miRNAs related to periodontitis [30,31], few have extensively analyzed EV-contained miRNAs. Although miRNAs enriched in EVs from LPS-stimulated THP-1 macrophage-like cells have been analyzed using RNA-seq [19], they differed significantly from the identified miRNAs. Notably, the transcription of miR155-5p during *Pg* infection was dependent on TLR2/NF- κ B signaling and independent of TLR4. Furthermore, seven out of the miRNAs upregulated within *Pg*-EVs might be regulated NF- κ B signaling because of harboring p65 binding sequences in their promoters. This suggests a potential dependence of miRNA composition into EVs on upstream innate immune signals. Single-cell RNA-seq analysis has reported increased expression of innate immune receptors across various cell types during periodontitis [1], indicating the potential secretion of distinct miRNAs during disease states compared to healthy conditions.

While the enhancement of miRNA transcription via innate immune signaling might contribute to altering the miRNA composition in EVs, this raises the question: Do all upregulated miRNAs undergo the enrichment within EVs? It has been reported that the composition of miRNAs within EVs differs significantly from that within cells, and the molecular characteristics of miRNAs (such as GC content, free energy, sequence motifs, and the activation state of host cells) may influence the miRNA composition within EVs [9–11]. The AGAGGG and GRGGSGC motifs that we identified exhibited similarity to previously reported sorting motifs [9], characterized by sequences of five to seven nucleotides with high G + C content. Additionally, it has been reported that the miRNA repertoire increased in EVs from K562 myelogenous leukemia cells contains the AGAGGG motif [11]. Since our study did not directly compare intracellular and EV miRNA profiles, we cannot conclude whether miRNA repertoires with AGAGGG motifs are preferentially sorted into *Pg*-EVs. However, considering the common detection of AGAGGG motif in miRNAs within EVs from leukemia cells like K562 and THP-1, it is plausible that miRNA repertoires with AGAGGG motif may have a propensity to be enriched within EVs from leukemia cells.

Certain miRNAs involved in intercellular crosstalk during infection may preferentially undergo enrichment within EVs, potentially contributing to the control of inflammation. The severity of periodontitis has been reported to correlate with the expression of IL-10 and IL-17 [32], suggesting that EV-containing miRNAs may regulate IL-10 expression. In this perspective, it is intriguing that miR-155, known as an inflammation-regulating factor, harbors the AGAGGG motif. Additionally, there is limited literature regarding the association of other miRNAs (hsa-mir-642a-3p, hsa-mir-671-5p, hsa-mir-3178, hsa-mir-3197, and hsa-mir-3616-3p) possessing AGAGGG and GRGGSGC motifs with *Pg* infection or periodontitis. The ErbB signaling pathway has been implicated in mucosal immunity, and disruption of EGF-EGFR interaction has been reported during *Pg* infection [33,34]. miR-642a and miR-3616, which harbor the AGAGGG motif, may be associated with ErbB signaling, potentially influencing mucosal immunity during *Pg* infection. These miRNAs may serve as novel biomarkers for periodontitis.

In conclusion, our study revealed that miRNAs profile concentrated within *Pg*-EVs and associated sequence motifs. Moreover, we indicated that the compositional alternation of miRNAs in *Pg*-EVs does not rely on TLR4 signaling but might be dependent on TLR2. These findings highlight the importance of innate immune receptor signaling in miRNA secretion during *Pg* infection. While we demonstrated that the enhanced transcription of miR-155 during *Pg* infection depends on TLR2 and NF- κ B, we did not explore how the composition of miRNAs in EVs changes upon inhibiting TLR2 or NF- κ B during *Pg* infection or by stimulating with TLR2 ligands. Additionally, future experimental investigations are

warranted to ascertain whether the AGAGGG and GRGGSGC motifs are involved in miRNA sorting or inflammation control. Such studies are expected to reveal the intricate pathogenesis of periodontitis.

Data availability

The microarray data supporting the findings of this study are available in the Gene Expression Omnibus (GEO) database under accession number GSE250449.

Ethical statement

Ethical approval is not required.

CRediT authorship contribution statement

Kayo Yoshida: data acquisition, Formal analysis, data interpretation, Writing – original draft. **Kaya Yoshida:** Conceptualization, study design, Supervision. **Yasuhiro Mouri:** Conceptualization, methodology-bioinformatics, Writing – review & editing, revising. **Ayu Takai:** data analysis. **Mariko Seyama:** data interpretation. **Mana Mekata:** data interpretation. **Noriko Mizusawa:** methodology-miRNA isolation and real-time PCR. **Keiko Miyoshi:** data interpretation, revising. **Yasusei Kudo:** data interpretation, revising. **Kazumi Ozaki:** Conceptualization, study design, supervision.

Declaration of competing interest

The authors declare no conflicts of interest associated with this study.

Acknowledgments

This study was supported by the Japan Society for the Promotion of Science (JSPS) Grants-in-Aid for Scientific Research (JSPS KAKENHI Grant Number JP23KJ1664), Grant-in-Aid for JSPS Fellows (Kayo Yoshida), and a Grant-in-Aid for Scientific Research from the Ministry of Education, Science, Sports, and Culture of Japan (20K21714) (Kaya Yoshida).

Appendix A. Supplementary data

Supplementary data to this article can be found online at <https://doi.org/10.1016/j.job.2024.04.001>.

References

- [1] Williams DW, Greenwell-Wild T, Brenchley L, Dutzan N, Overmiller A, Sawaya AP, et al. Human oral mucosa cell atlas reveals a stromal-neutrophil axis regulating tissue immunity. *Cell* 2021;184:4090–104.
- [2] Zhou X, Xie F, Wang L, Zhang L, Zhang S, Fang M, et al. The function and clinical application of extracellular vesicles in innate immune regulation. *Cell Mol Immunol* 2020;17:323–34.
- [3] Cai R, Wang L, Zhang W, Liu B, Wu Y, Pang J, et al. The role of extracellular vesicles in periodontitis: pathogenesis, diagnosis, and therapy. *Front Immunol* 2023;14:1151322.
- [4] Yoshida K, Yoshida K, Fujiwara N, Seyama M, Ono K, Kawai H, et al. Extracellular vesicles of *P. gingivalis*-infected macrophages induce lung injury. *Biochim Biophys Acta, Mol Basis Dis* 2021;1867:166236.
- [5] Bartel DP. MicroRNAs: target recognition and regulatory functions. *Cell* 2009;136:215–33.
- [6] Mori MA, Ludwig RG, Garcia-Martin R, Brandão BB, Kahn CR. Extracellular miRNAs: from biomarkers to Mediators of Physiology and disease. *Cell Metab* 2019;30:656–73.
- [7] Li Y, Tan J, Miao Y, Zhang Q. MicroRNA in extracellular vesicles regulates inflammation through macrophages under hypoxia. *Cell Death Discov* 2021;7:285.
- [8] Alexander M, Hu R, Runtsch MC, Kagele DA, Mosbrugger TL, Tolmacheva T, et al. Exosome-delivered microRNAs modulate the inflammatory response to endotoxin. *Nat Commun* 2015;6:7321.
- [9] Garcia-Martin R, Wang G, Brandão B, Zanotto TM, Shah S, Patel SK, et al. MicroRNA sequence codes for small extracellular vesicle release and cellular retention. *Nature* 2022;601:446–51.

- [10] Squadrito ML, Baer C, Burdet F, Maderna C, Gilfillan GD, Lyle R, et al. Endogenous RNAs modulate MicroRNA sorting to exosomes and transfer to acceptor cells. *Cell Rep* 2014;8:1432–46.
- [11] Gao X, Wan Z, Wei M, Dong Y, Zhao Y, Chen X, et al. Chronic myelogenous leukemia cells remodel the bone marrow niche via exosome-mediated transfer of miR-320. *Theranostics* 2019;9:5642–56.
- [12] Liu T, Zhang Q, Zhang J, Li C, Miao Y, Lei Q, et al. EVmiRNA: a database of miRNA profiling in extracellular vesicles. *Nucleic Acids Res* 2019;47:D89–93.
- [13] Wang W, Yue C, Gao S, Li S, Zhou J, Chen J, et al. Promising roles of exosomal microRNAs in systemic Lupus Erythematosus. *Front Immunol* 2021;12:757096.
- [14] Xu H, Du X, Xu J, Zhang Y, Tian Y, Liu G, et al. Pancreatic β cell microRNA-26a alleviates type 2 diabetes by improving peripheral insulin sensitivity and preserving β cell function. *PLoS Biol* 2020;18:e3000603.
- [15] Kimura K, Hohjoh H, Fukuoka M, Sato W, Oki S, Tomi C, et al. Circulating exosomes suppress the induction of regulatory T cells via let-7i in multiple sclerosis. *Nat Commun* 2018;9:17.
- [16] Festing MF. On determining sample size in experiments involving laboratory animals. *Lab Anim* 2018;52(4):341–50.
- [17] Wu P, Feng J, Wang W. Expression of miR-155 and miR-146a in the saliva of patients with periodontitis and its clinical value. *Am J Transl Res* 2021;13:6670–7.
- [18] Dede FÖ, Gökmenoğlu C, Türkmen E, Doğan ŞB, Ayhan BS, Yıldırım K. Six miRNA expressions in the saliva of smokers and non-smokers with periodontal disease. *J Periodontal Res* 2023;58:195–203.
- [19] Chen L, Yao X, Yao H, Ji Q, Ding G, Liu X. Exosomal miR-103-3p from LPS-activated THP-1 macrophage contributes to the activation of hepatic stellate cells. *FASEB J* 2020;34:5178–92.
- [20] Maekawa T, Krauss JL, Abe T, Jotwani R, Triantafilou M, Triantafilou M, et al. *Porphyromonas gingivalis* manipulates complement and TLR signaling to uncouple bacterial clearance from inflammation and promote dysbiosis. *Cell Host Microbe* 2014;15:768–78.
- [21] Wielento A, Bereta GP, Łagosz-Ćwik KB, Eick S, Lamont RJ, Grabiec AM, et al. TLR2 activation by *Porphyromonas gingivalis* requires both PPAD activity and fimbriae. *Front Immunol* 2022;13:823685.
- [22] Burns E, Eliyahu T, Uematsu S, Akira S, Nussbaum G. TLR2-dependent inflammatory response to *Porphyromonas gingivalis* is MyD88 independent, whereas MyD88 is required to clear infection. *J Immunol* 2010;184:1455–62.
- [23] Thompson RC, Vardinogiannis I, Gilmore TD. Identification of an NF- κ B p50/p65-responsive site in the human MIR155HG promoter. *BMC Mol Biol* 2013;14:24.
- [24] Park MH, Park E, Kim HJ, Na HS, Chung J. *Porphyromonas gingivalis*-induced miR-132 regulates TNF α expression in THP-1 derived macrophages. *SpringerPlus* 2016;5:761.
- [25] Coenen-Stass AML, Pauwels MJ, Hanson B, Perez CM, Conceição M, Wood MJA, et al. Extracellular microRNAs exhibit sequence-dependent stability and cellular release kinetics. *RNA Biol* 2019;16:696–706.
- [26] Ho J, Moyes DL, Tavassoli M, Naglik JR. The role of ErbB receptors in infection. *Trends Microbiol* 2017;25:942–52.
- [27] Daily ZA, Al-Ghurabei BH, Al-Qarakhli AMA, Moseley R. MicroRNA-155 (miR-155) as an accurate biomarker of periodontal status and coronary heart disease severity: a case-control study. *BMC Oral Health* 2023;23:868.
- [28] O'Connell RM, Taganov KD, Boldin MP, Cheng C, Baltimore D. MicroRNA-155 is induced during the macrophage inflammatory response. *Proc Natl Acad Sci U S A* 2007;104:1604–9.
- [29] Taganov KD, Boldin MP, Chang K, Baltimore D. NF- κ B-dependent induction of microRNA miR-146, an inhibitor targeted to signaling proteins of innate immune responses. *Proc Natl Acad Sci U S A* 2006;103:12481–6.
- [30] Gao X, Zhao D, Han J, Zhang Z, Wang Z. Identification of microRNA-mRNA-TF regulatory networks in periodontitis by bioinformatics analysis. *BMC Oral Health* 2022;22:118.
- [31] Liu L, Chen Y, Wang L, Yang F, Li X, Luo S, et al. Dissecting B/Plasma cells in periodontitis at single-cell/Bulk Resolution. *J Dent Res* 2022;101:1388–97.
- [32] Sun L, Girmay M, Wang L, Jiao Y, Zeng E, Mercer K, et al. IL-10 Dampens an IL-17-mediated periodontitis-associated inflammatory network. *J Immunol* 2020;204:2177–91.
- [33] Ciaston I, Budziaszek J, Satala D, Potempa B, Fuchs A, Rapala-Kozik M, et al. Proteolytic activity-independent activation of the immune response by gingipains from *Porphyromonas gingivalis*. *mBio* 2022;13:e0378721.
- [34] Pyrc K, Milewska A, Kantyka T, Sroka A, Maresz K, Koziel J, et al. Inactivation of epidermal growth factor by *Porphyromonas gingivalis* as a potential mechanism for periodontal tissue damage. *Infect Immun* 2013;81:55–64.